Surface enhanced Raman spectroscopy on a flat graphene surface

Weigao Xu[a], Xi Ling[a], Jiaqi Xiao[a], Mildred S. Dresselhaus[b,c], Jing Kong[b], Hongxing Xu[d], Zhongfan Liu[a], and Jin Zhang[a,1]

[a]Center for Nanochemistry, Beijing National Laboratory for Molecular Sciences, Key Laboratory for the Physics and Chemistry of Nanodevices, State Key Laboratory for Structural Chemistry of Unstable and Stable Species, College of Chemistry and Molecular Engineering, Peking University, Beijing 100871, China; [b]Department of Electrical Engineering and Computer Science, Massachusetts Institute of Technology, Cambridge, MA 02139; [d]Beijing National Laboratory of Condensed Matter Physics, Institute of Physics, Chinese Academy of Sciences, Beijing 100190, China; and [c]Department of Physics, Massachusetts Institute of Technology, Cambridge, MA 02139

Surface enhanced Raman spectroscopy (SERS) is an attractive analytical technique, which enables single-molecule sensitive detection and provides its special chemical fingerprints. During the past decades, researchers have made great efforts towards an ideal SERS substrate, mainly including pioneering works on the preparation of uniform metal nanostructure arrays by various nanoassembly and nanotailoring methods, which give better uniformity and reproducibility. Recently, nanoparticles coated with an inert shell were used to make the enhanced Raman signals cleaner. By depositing SERS-active metal nanoislands on an atomically flat graphene layer, here we designed a new kind of SERS substrate referred to as a graphene-mediated SERS (G-SERS) substrate. In the graphene/metal combined structure, the electromagnetic "hot" spots (which is the origin of a huge SERS enhancement) created by the gapped metal nanoislands through the localized surface plasmon resonance effect are supposed to pass through the monolayer graphene, resulting in an atomically flat hot surface for Raman enhancement. Signals from a G-SERS substrate were also demonstrated to have interesting advantages over normal SERS, in terms of cleaner vibrational information free from various metal-molecule interactions and being more stable against photo-induced damage, but with a comparable enhancement factor. Furthermore, we demonstrate the use of a freestanding, transparent and flexible "G-SERS tape" (consisting of a polymer-layer-supported monolayer graphene with sandwiched metal nanoislands) to enable direct, real time and reliable detection of trace amounts of analytes in various systems, which imparts high efficiency and universality of analyses with G-SERS substrates.

atomically smooth substrate | metal-molecule isolation | signal fluctuation | mediator | application

For almost all sorts of analytical methods, the dream to improve their sensitivity as well as their reproducibility and to optimize the analytical process (e.g., to simplify the sample preparation/measurement procedures for quick analysis and to enable in situ and real time monitoring) is a long-term pursuit. Spectroscopic approaches based on fluorescence, infrared absorption and Raman scattering have been developed with rising importance for various sensing and imaging applications. Among them, Raman scattering provides more structural information (characteristic vibrational information of each chemical bond) over fluorescence, and higher spatial resolution (shorter excitation wavelength) over infrared absorption (1). However, as Raman scattering is an inelastic scattering process with a very low cross-section, it is not very sensitive and thus has limited analysis efficiency and applicability.

Because of this, surface enhanced Raman spectroscopy (SERS) has been developed since the 1970s (2–4) to enable ultrasensitive characterization down to the single-molecule level (5, 6), comparable to single-molecule fluorescence spectroscopy (7). In a SERS experiment, a rough metal surface or colloidal metal nanostructures are typically used. Here, the highly curved or gapped metal regions (under proper incident light conditions)

give rise to greatly enhanced local electromagnetic fields via the localized surface plasmon resonance effect. The localized electromagnetic field (usually called a "hot" spot) thus results in the dominant contribution of SERS enhancement [referred to as electromagnetic enhancement (EM)], which can reach 10^8 or more (8–10). Usually there is another chemical contribution called chemical enhancement (CM), but with a minor enhancement factor (typically 10 to 10^2) (11, 12). As a result, molecules adsorbed near the electromagnetic hot spots dominate the Raman intensity. The distribution of molecules on a normal SERS substrate is usually complicated, as the molecules near the hot spots can be in fluctuating amounts and random orientations. On the other hand, chemical interactions between the molecules and the metal substrate can make this case more complicated. Chemical adsorption-induced vibrations, molecular deformation and distortion, charge transfer between the metal and molecules, photocarbonization, photobleaching or metal-catalyzed side reactions (10, 13) may all affect the final signal and make it difficult to precisely assign each vibration of a SERS spectrum. Thus, the SERS signal is sometimes too sensitive to a SERS substrate, possible fluctuations caused by nonuniform molecular adsorption (amounts/configurations), different metal enhancers and the corresponding metal-molecule interactions bring down the comparability between parallel SERS experiments, and as a result standard analytical methods based on SERS have been rarely popularized. To further understand the SERS effect and fully excite its advanced applications, a SERS substrate with a more "intelligent" form is still lacking.

From the above, the availability of an enhancement substrate, which can give a uniform, stable, clean and highly sensitive SERS response has remained a bottleneck for extending the further applications of SERS (10, 14). Current efforts towards more reproducible SERS analyses are mainly focused on the nanotailoring or nanoassembly of substrates with uniform metal nanostructure arrays (15–19). However, a "uniform" SERS substrate is still not uniform on the nanoscale, the distribution of molecules and their states may be quite uncontrollable in the vicinity of the electromagnetic hot spots. On the other hand, metal nanoparticles with a thin and inert SiO_2 shell were recently demonstrated to make SERS signals cleaner (13). Yet, the coating of a pinhole-free and thin SiO_2 layer (to avoid metal-molecule interaction without large sacrifice to the SERS-activity) is an over delicate technique. In this work, based on the use of the two-dimensional atomic crystal graphene, we designed a unique kind of SERS
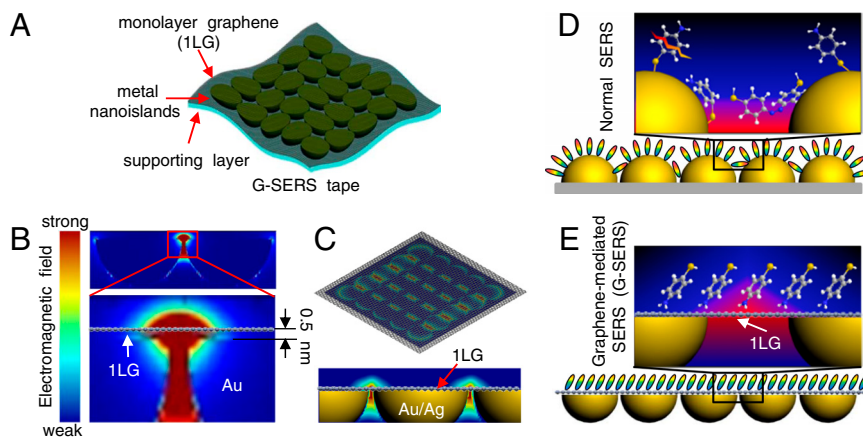
CHEMISTRY

Fig. 1. Design of a G-SERS substrate. (*A*) Components of a G-SERS tape. (*B*) The simulated electromagnetic field distribution of a 60-nm gold hemisphere dimer covered with graphene (with a 2-nm gap between two gold hemispheres and a 0.5-nm gap between gold hemispheres and graphene). The excitation wavelength is 632.8 nm, with the incident direction perpendicular to the graphene surface (from top to bottom). (*C*) The resulting "hot" graphene surface to serve as a G-SERS substrate. (*D*, *E*) Schematic illustration of molecules adsorbed on a normal SERS substrate (*D*) and on a G-SERS substrate (*E*).

substrate containing a graphene/metal-combined structure, referred to as a graphene-mediated SERS (G-SERS) substrate.

Results

As illustrated in Fig. 1, the active surface of our G-SERS substrate is a monolayer graphene (1LG), with gold/silver nanoislands tightly adhered on the backside. By collecting electromagnetic hot spots from the metal nanoislands on a graphene surface, a G-SERS substrate is anticipated to offer an atomically smooth surface for controllable molecular arrangements as well as well-defined molecular interactions, yet also has the electromagnetic hot spots created by the localized surface plasmon resonance of gold or silver nanoislands adhered on the backside of graphene.

In a G-SERS substrate, the metal nanoislands focus the incident laser, creating localized electromagnetic hot spots close to the graphene surface. The permeability of the electromagnetic field to pass through the graphene is critical for the final enhancement activity. First, theoretical calculations are carried out. For simplicity, two 60-nm diameter gold hemispheres adhering below a monolayer graphene are used to simulate a G-SERS substrate. From the three dimensional finite difference time domain (3D-FDTD) simulations results as shown in Fig. 1*B*, localized electromagnetic field occurs at the gap of the hemisphere dimer, spreads from the central strongest hot spot to the vicinity (The permeability was also supported by extended Mie theory calculations of a graphene-coated 60-nm gold sphere dimer, *SI Appendix*, Fig. S1). By comparing with that of gold hemispheres without graphene, we find that graphene exhibits good permeability for the electromagnetic hot spot to pass through, and interestingly the maximum $|E_{loc}/E_0|^2$ is even almost one time stronger (*SI Appendix*, Fig. S2). These results encouraged us that the close vicinity of these hot spots from metal nanostructures can make the monolayer graphene a hot surface (Fig. 1*C*), and thus allows localized electromagnetic enhancement to be achieved on an atomically flat surface.

Fig. 1*D* and 1*E* illustrate possible states of molecules adsorbed on a normal SERS substrate (Fig. 1*D*) and a G-SERS substrate (Fig. 1*E*). In Fig. 1*D*, molecules are in various orientations according to the morphology of the metal nanoislands. The enlarged view in Fig. 1*D* illustrates various possibilities that may make the enhanced Raman signals complicated. In contrast, by taking the flat and hot graphene surface as the Raman enhancer, as illustrated in Fig. 1*E*, the strong Raman enhancement from localized electromagnetic hot spots created by metal nanoislands can be realized on an atomically smooth surface. The monolayer graphene is expected to act as a multifunctional "SERS mediator", including: (*i*) a flat supporting surface to arrange molecules

in a more controllable way, (*ii*) a spacer to separate the metal-molecule contact, (*iii*) additional effects like a stabilizer of both the substrate and the molecules under laser exposure.

To seek the possible superiorities of a G-SERS substrate, a rational way was used to fabricate substrates with both G-SERS regions and normal SERS regions for comparison. As shown in Fig. 2*A*, a uniform layer of molecules, such as rhodamine 6G (R6G) or copper phthalocyanine (CuPc), were first deposited on a SiO$_2$/Si substrate by vacuum thermal evaporation. Mechanically exfoliated graphene pieces were then transferred to the top of the molecules, creating regions with and without graphene (for regions without graphene, our Raman inspections were carried out only on those regions that are not touched by the adhesive scotch tape used in the mechanical exfoliation, to make sure no damage was done to the Raman probes). Finally, gold or silver nanoislands adhering to the graphene were constructed by vacuum thermal evaporation of an 8-nm metal film (a preferred thickness for gold as illustrated in *SI Appendix*, Figs. S3 and S4) on the top of both regions (1LG and the bare substrate). It should be pointed out that gold and silver are the most popular electromagnetic enhancers, where gold is more stable but the enhancement is usually less than that for silver. Silver is more likely to be affected by the environment, such as oxidation processes which will decrease the enhancement over time. Here we show that both of gold and silver can be used effectively for the fabrication of a G-SERS substrate. The method of vacuum thermal evaporation can avoid external contaminations such as surfactants which would be introduced by using nanostructures prepared by colloidal methods (20). Thus, G-SERS and normal SERS regions (defined as G-SERS(M) and SERS(M), where M is the metal used as the electromagnetic enhancer) were constructed corresponding to the regions with and without graphene, respectively.

Typical Raman spectra of R6G with G-SERS(Au), G-SERS(Ag), SERS(Au), and SERS(Ag) are shown in Fig. 2*B* from bottom to top, respectively. First, it can be seen that the G-SERS regions give more reproducible and cleaner signals as compared to normal SERS. For G-SERS(Au) and G-SERS(Ag), the spectral features are the same as one another, with clear peaks at 612, 635, 660, 771, 1181, 1313, 1361, 1511, 1648 cm^{-1} (± 1 cm^{-1}) (see *SI Appendix*, Table S1). The peaks at around 1570 and 2625 cm^{-1} (marked by *) are the G-band and G′-band of monolayer graphene, respectively. The relative intensity of the graphene peak as compared to R6G is different in G-SERS(Au) and G-SERS(Ag) (this variability is reproducible from sample to sample in our parallel measurements); this may be because of a different chemical contribution of gold and silver. In contrast, Raman spectra enhanced by SERS(Au) and SERS(Ag) show many additional
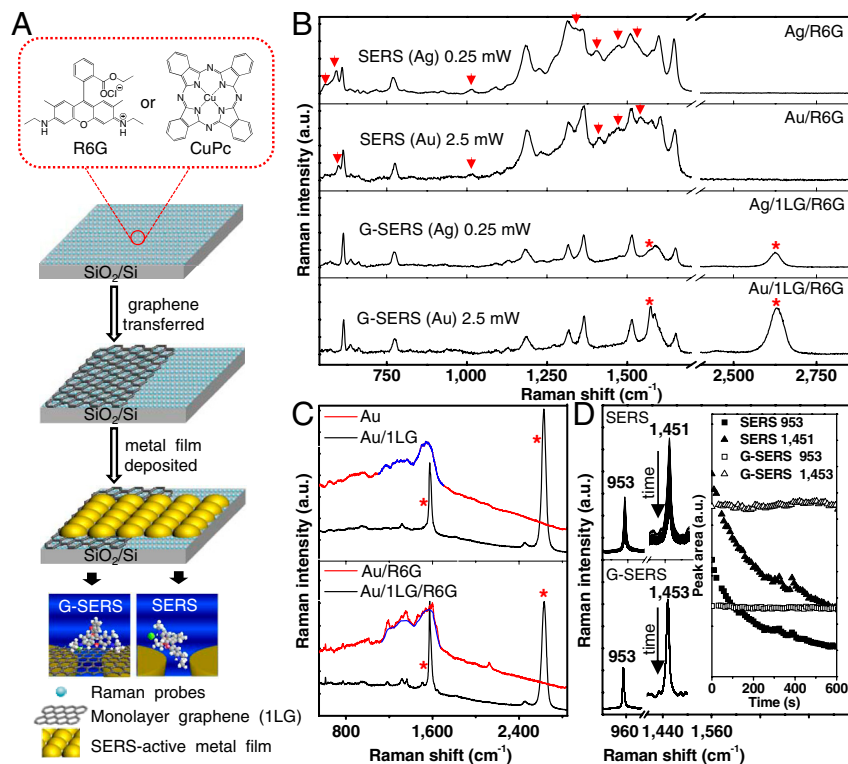
Fig. 2. Comparison of signals from a G-SERS substrate and a normal SERS substrate. (*A*) Schematic route for sample preparation with G-SERS and SERS regions on a SiO$_2$/Si substrate. An enlarged view shows the chemical structure of the probe molecules used in the experiment. (*B*) SERS and G-SERS spectra of R6G with gold and silver nanoislands used as an electromagnetic enhancer, respectively. Red arrows here point to additional and nonreproducible peaks in spectra of normal SERS. (*C*) Photocarbonization effect (which causes a background at $1100 \sim 1700$ cm^{-1}) in SERS and G-SERS substrates. (*D*) Stability of the SERS (top) and G-SERS (bottom) spectra of CuPc in a time series of 600 s. The inset shows the integrated intensity of the peaks (at 953, 1451 cm^{-1} for SERS, and 953, 1453 cm^{-1} for G-SERS, respectively) change with the increased acquisition time. Time sequence: from top to bottom. "*" in *B* and *C* marks the G-band ($\sim$1570 cm^{-1}) and G'-band ($\sim$2625 cm^{-1}) of 1LG. G-SERS spectra are measured under the same conditions with the corresponding SERS spectra and are shown on the same intensity scale, except for C (bottom), where the SERS spectrum was acquired under a 10% laser power compared to the G-SERS spectrum.

peaks (as marked by red arrows) compared to the G-SERS results. Among these additional peaks, such as at 597, 1014, 1411, 1468, 1540 cm^{-1} in SERS(Au) and 554, 590, 1012, 1336, 1403, 1471, 1531 cm^{-1} in SERS(Ag), some of them may be from contamination of surface carbons (as will be described below), some are new emerging bands possibly due to the modified surface selection rules (because of alteration of the symmetry of the vibrational modes under changed configurations), while others remain difficult to assign precisely. Parallel measurements are demonstrated and we found that these additional signals are irreproducible (see *SI Appendix,* Fig. S6). When looking at those bands, which are also observed in the G-SERS spectra, many bands are shifted (probably due to a charge-transfer effect of the metal-R6G), and the amount of shifts are different for SERS(Au) and SERS(Ag). Thus, the SERS results will depend on various factors, which may result in the appearance and disappearance of various features, mixed with peaks having up or down shifted frequencies. As a result, it would be almost impossible to assign each vibration precisely, since the spectral features are no longer clearly dependent on the primary structure of the sample molecules.

Additionally, we also found that graphene makes the SERS system more stable. Photo-induced damage is a common characteristic of SERS, and is popularly known as photocarbonization and photobleaching. Raman spectra of the as prepared G-SERS and SERS substrates (without molecules) are shown in Fig. 2*C*, top panel. First, one can see that the G-SERS substrate provides a cleaner baseline than that of normal SERS: The photocarbonization background in the $1100 \sim 1700$ cm^{-1} range (marked in blue line) for the SERS spectra is not observed in the G-SERS spectra, together with the emergence of a characteristic signal of monolayer graphene. Because no Raman probes were introduced here, this carbonization background is normally considered to be due to surface carbon-based adsorbates from the atmosphere. In fact, the photocarbonization of adsorbates was observed and studied soon after the SERS effect was discovered (21), but so far this signal contamination problem has not yet been resolved. This photocarbonization effect will be even more pronounced in an

actual SERS measurement when probe molecules are present. As shown in Fig. 2*C* (bottom), even with a much lower laser power (the SERS spectrum is acquired under a 10% laser power compared to G-SERS), the SERS spectrum of R6G shows an obvious photocarbonization background (marked in blue line) while this background is absent in the G-SERS spectrum. The presence of graphene cover layer may suppress the catalytic activity of the gold nanoislands and prevent the photo-induced carbonization, as well as keep R6G molecules from direct contact with the gold film, thus preventing adsorbates (from the atmosphere) and R6G molecules from photocarbonization. The high thermal conductivity of graphene may also partly contribute to the enhanced stability, and actually we have found that the morphology of the metal film changes after a relatively large laser power exposure if there is no graphene layer present, while it keeps stable for the G-SERS regions. An additional effect, the lower photoluminescence background in a G-SERS substrate than that of normal SERS, is consistent with the reported results that graphene is an effective quencher for both the fluorescence of dyes (22, 23) and the photoluminescence of a gold film, through a resonance energy transfer process (24).
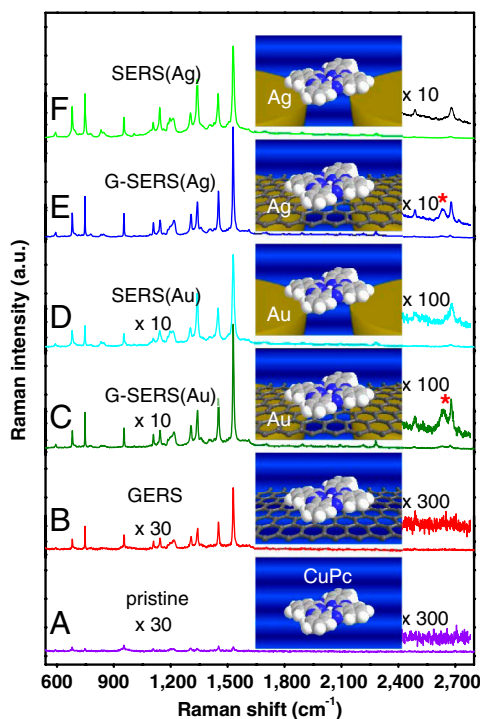
On the other hand, the photobleaching (or photodegradation) of the Raman probes induced by the laser is also a well-known feature in normal SERS experiments, especially for dyes. During a normal SERS measurement, the intensity of the Raman signals of molecules may decrease with increased acquisition time (especially under a high laser power), and this effect will lead to a variation of the Raman spectra with acquisition time and laser power. Fig. 2*D* shows a comparison of the stability of the Raman spectra of CuPc of SERS(Au) (top) and G-SERS(Au) (bottom) regions. It is seen here that the signal of CuPc in the normal SERS region decreases quickly in intensity during a 600 s measurement while in the G-SERS region it remains totally stable. It is speculated that both the separation of CuPc from the rough gold film and the formation of a graphene/CuPc complex through π-π interactions may contribute to the stability of CuPc.

The above results in Fig. 2 suggest that, in a G-SERS substrate (when the rough metal substrate is replaced by a hot and atom-

ically flat graphene surface), Raman enhancement turns out to be cleaner (with characteristic and reproducible vibrational modes in which fluctuating information is removed) and more stable (against laser-induced damage such as photocarbonization and photobleaching). It should be emphasized that the above characteristics of a normal SERS substrate do not mean shortcomings of the SERS technique itself, and actually it oppositely reflects the fascinating capability of SERS (even capable of monitoring the actions of a single molecule). However, currently the state of the art of SERS is still mostly limited to the study of a mixture of molecules in unclear states with poor controllability. Thus, the G-SERS substrate is anticipated to act as an effective tool to implement SERS, both for general analyses (with better controllability and reproducibility among parallel measurements) and for many advanced applications.

Further, we checked the enhancement factor of G-SERS substrates. For comparison, the Raman spectra of CuPc (pristine), 1LG/CuPc [graphene-enhanced Raman scattering (25), "GERS"], Au/CuPc [SERS(Au)], Au/1LG/CuPc [G-SERS(Au)], Ag/CuPc [SERS(Ag)], and Ag/1LG/CuPc [G-SERS(Ag)] are shown in Fig. 3(A–F). All the spectra are acquired under the same conditions and all the spectra are shown with the same intensity scale, where the Raman signal data is multiplied by 30 in the case of the pristine and GERS and by 10 in the case of G-SERS(Au) and SERS (Au). Here, the relative intensity of the graphene signal seems much lower (the G-band of graphene is almost invisible but the G′-band can still be clearly distinguished) as compared to measurement of R6G in Fig. 2B, and this is because of a resonance Raman enhancement effect of CuPc under our measurement condition (632.8 nm). Through the integrated area of the
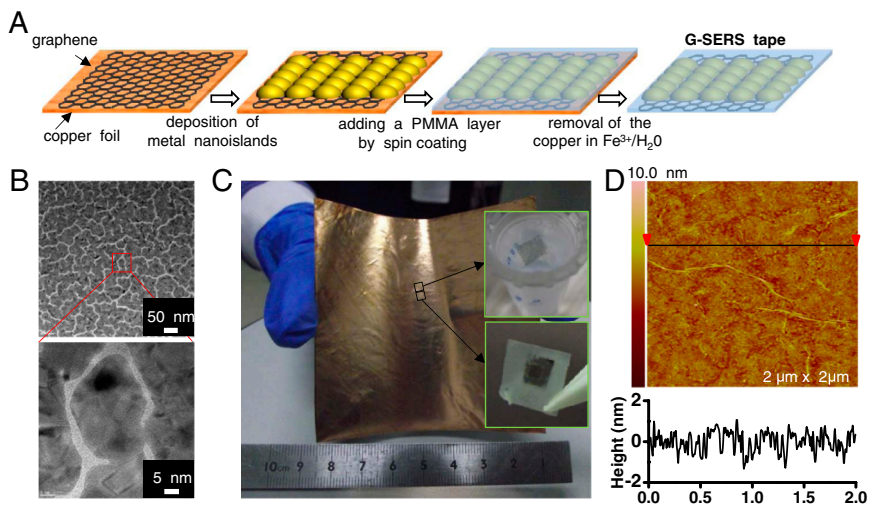
1530 cm^{-1} peak, taking the pristine spectra as a reference, it is enhanced by a factor of 14 for GERS, 61 for SERS(Au), 85 for G-SERS(Au), 580 for SERS(Ag), and 755 for G-SERS(Ag). It should be noted that here the enhancement factors for the SERS region and the G-SERS region are both seriously undervalued since the absorption of the metal film makes only molecules at the gaps between the metal nanoislands (of course, this is quite a minority) contribute to their final signal intensity. However, here it is fair to compare the relative sensitivity between a normal SERS substrate and a G-SERS substrate. The weak signal of pristine CuPc is magnified, and under the measurement conditions (632.8 nm excitation), silver is a better electromagnetic enhancer than gold. Most importantly, for both the case of gold and silver, the enhancement factors of the G-SERS regions are even slightly higher than those of normal SERS for most of the bands. This means that the presence of the graphene layer will not cause the localized electromagnetic field to decay observably in its vicinity, which is consistent with our theoretical results as mentioned before. The small enhancement of the graphene substrate is consistent with our earlier results (25, 26), possibly due to a chemical enhancement. By a careful comparison of their spectral features, it can be seen that the spectral feature from a G-SERS substrate remains the same as that from a graphene substrate while the enhancement was greatly improved by the introduction of the electromagnetic enhancement. Consistent results can be observed from the signals of R6G from a G-SERS substrate and a graphene substrate as shown in Table S1 (*SI Appendix*), regardless of the material of the metal enhancer. Thus, by collecting hot spots of metal nanoislands on a flat graphene surface, G-SERS substrate provides comparable sensitivity with that of normal SERS. The better-defined molecule-substrate interactions in a G-SERS substrate is also intriguing, as an atomically compact and chemically inert graphene surface seems to cut down signal fluctuations among different metal enhancers.

A "universal" substrate should be sufficiently economical, sufficiently convenient, and sufficiently compatible with various samples in a different state. As described in the following, we developed a general type of G-SERS substrate (which we call a "G-SERS tape"), which is transparent, freestanding, and flexible (by virtue of the high light transmittance and good flexibility of both graphene and the selected polymer). As a schematic representation in Fig. 1A, a G-SERS tape consists of three parts: monolayer graphene, a polymer supporting layer, and sandwiched metal nanoislands adhering to the backside of the active face of graphene. Fabrication of G-SERS tapes and their applications in various situations, including surfaces with arbitrary morphology, or even directly on a solution surface are demonstrated. Such a G-SERS process does not require special sample preparation, is a noninvasive process, and is very convenient for in situ characterization or real time monitoring.

As shown in Fig. 4A, taking the G-SERS(Au) tape as example, an 8-nm gold film was first deposited on a large area monolayer graphene grown on a 8×8 cm^2 copper foil [prepared by the chemical vapor deposition method (27)], which is uniform with high quality (see *SI Appendix*, Fig. S7). A poly(methyl methacrylate) (PMMA) film, which is optically transparent, inert, and Raman inactive, was then fabricated by spin-coating and dried at 170 °C for 30 min (27, 28). Finally, a transparent, freestanding, and flexible G-SERS tape with a PMMA/metal/graphene structure was obtained by etching the copper foil in a FeCl$_3$/H$_2$O solution. This technique is suitable for scaled production of G-SERS tapes (Fig. 4C). The transmission electron microscopy (TEM) image in Fig. 4B shows the morphology of an 8-nm gold film, in which most gaps between the nanoislands are $2 \sim 3$ nm, thereby allowing for a considerable electromagnetic enhancement. As shown in Fig. 4D, the atomic force microscopy characterization shows that the active side (graphene side) of the G-SERS tape is flat, with a fluctuation (surface roughness) along the film length of less than ± 2 nm.

Fig. 3. Comparison of the Raman spectra of CuPc with different enhancement methods. (A) Pristine spectrum: CuPc/SiO$_2$/Si. (B) GERS spectrum: 1LG/CuPc/SiO$_2$/Si. (C, D) G-SERS (Au/1LG/CuPc/SiO$_2$/Si) (C) and SERS (Au/CuPc/SiO$_2$/Si) (D) spectra of CuPc with Au as the electromagnetic enhancer. (E, F) G-SERS (Ag/1LG/CuPc/SiO$_2$/Si) (E) and SERS (Ag/CuPc/SiO$_2$/Si) (F) spectra of CuPc with Ag as the electromagnetic enhancer. In A and B the spectra were magnified by a factor of 30. In C and D the spectra were magnified by a factor of 10. Inset pictures are the corresponding sample structures that represent different enhancement methods. An enlarged view of the regions at 2400 ∼ 2720 cm^{-1} (including the G′-band of 1LG) is also shown, with G′-band of 1LG marked by "*".

Xu et al.

Fig. 4. Transparent, freestanding and flexible G-SERS tape prepared from CVD-grown monolayer graphene. (*A*) Schematic steps of the preparation route. (*B*) TEM images of an 8-nm gold film with a global view (top) and an enlarged view (bottom), showing that most gaps are on the size of 2 ∼ 3 nm. (*C*) Photograph of an 8×8 cm^2 G-SERS substrate before the removal of copper. Insets on the right are two freestanding G-SERS(Au) tapes, one is floating on water (top) and the other is held with tweezers (supported by a windowed scotch tape) (bottom), respectively. (*D*) Atomic force microscopy image of the graphene side of a G-SERS(Au) tape (top), together with a section analysis on the bottom. This indicates that the surface of the resulting G-SERS tape is flat, with a height fluctuation of less than ±2 nm.

Mechanically exfoliated graphene is also suitable for use in fabricating G-SERS tapes (see *SI Appendix*, Fig. S8). A G-SERS tape with silver as an electromagnetic enhancer [G-SERS(Ag) tape)] are prepared through a similar procedure (with a few modifications) and this tape is also described in the *SI Appendix*. As the active metal is buried inside the graphene and the PMMA layer (in the case of Ag, there is an additional protection layer) without exposure to the atmosphere, it is anticipated that these G-SERS tapes could have a long shelf life. Because of the flexibility of a G-SERS tape, the contact between the tape and the target material will be good enough to achieve the G-SERS enhancement.

Fig. 5 shows several typical analyses. As shown in Fig. 5*A*, G-SERS tapes shown in Fig. 4 can be used directly for real time analysis of samples in an aqueous solution, where we first put such a G-SERS tape floating on water, and a clean baseline was obtained with a clear graphene signal. Next, the same G-SERS tape was placed on a 1×10^{-5} M aqueous solution of R6G, and the intrinsic signal of R6G appeared in the Raman spectra (with the same spectral features as the G-SERS results in Fig. 2*B*). Additionally, the R6G signal disappeared after washing and replacing the G-SERS tape on water. This reversibility suggests that G-SERS tape may be exploited in real time sensing processes, such as online monitoring of water contaminants. Furthermore, the Raman spectra of a self-assembled monolayer of *p*-aminothiophenol on a flat gold surface (Fig. 5*B*) and of CuPc molecules adsorbed on a cauliflower surface (Fig. 5*C*) shows that G-SERS tapes can be used for the analysis of trace amounts of molecules on any surface with arbitrary morphology. Moreover, we extend G-SERS measurements to other solvents like ethanol by making a small modification to the G-SERS tape (see *SI Appendix*, Fig. S13). Therefore, this kind of G-SERS substrate is widely applicable for direct, noninvasive and ultrasensitive Raman measurements, including real time monitoring on a solution surface and on other surfaces with any arbitrary morphology.

Discussion

SERS is a powerful tool and it can be more powerful when exploited with a carefully designed substrate. Among the wide researches on SERS during the past years, great efforts have been made towards gaining a theoretical understanding of the enhancement mechanism (4, 29, 30) and resulting in extended practical applications (13, 31–33). The basic physical characteristic that a localized surface plasmon resonance (the origin of a large SERS enhancement) occurs only at those closely gapped or highly curved plasmonic metal nanostructures has hindered the SERS technique from being used on a flat surface. In this report, we demonstrated a G-SERS substrate in which a plasmonic metal

nanoisland array is adhered to a graphene surface, creating an atomically smooth surface with strong electromagnetic hot spots that can be used for Raman enhancement. The concept of enhancing the Raman signals on a flat graphene surface simplifies the
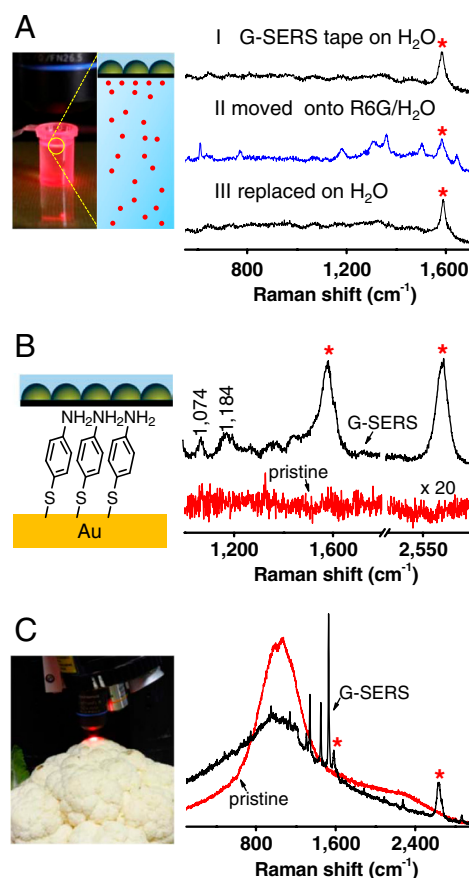
Fig. 5. Analyzing trace amounts of molecules under a variety of situations using the transparent, freestanding and flexible G-SERS(Au) substrate. (*A*) A real time and reversible G-SERS characterization of R6G directly in a 1×10^{-5} M aqueous solution. (I, II, III are the Raman spectra with the same G-SERS tape on H$_2$O, R6G/H$_2$O and replaced on H$_2$O, respectively). (*B*) Pristine (red line) and G-SERS (black line) measurements of a self-assembled monolayer of *p*-aminothiophenol on a flat gold surface. (*C*) Pristine (red line) and G-SERS (black line) measurements of a cauliflower surface with adsorbed CuPc (by soaking in a 1×10^{-5} M CuPc solution in ethanol for 10 min). "*" marks the enhanced G-band and G'-band features of 1LG. Sample structures are shown in the left insets.

Xu et al.

CHEMISTRY

determination of the precise amount of molecules, their detailed position and orientation information, as well as the molecule-substrate interaction. The characteristic Raman signal and atomically precise amount of graphene also make it a natural internal standard. G-SERS substrates are anticipated to be exploited in many fields, such as reliable qualitative and label-free quantitative detection, and the characterization of intrinsic structural information from samples without the introduction of spurious spectral features coming from metal contamination.

In conclusion, by introducing plasmonic metal to a graphene layer, an atomically flat substrate for SERS was developed. Cleaner and more reproducible signals were obtained with a comparable enhancement factor. The use of a transparent, freestanding and flexible G-SERS tape also opens up opportunities for more challenging applications such as direct, noninvasive and online analyses for samples in various states. G-SERS substrate shows a unique application of graphene and it is anticipated to benefit both the deeper understanding of the SERS effect itself and various practical applications of SERS.

Materials and Methods

Mechanically exfoliated graphene was prepared from Kish graphite (Covalent Materials Corp.) using Scotch tape on a $SiO_2(300 \text{ nm})/Si$ substrate (34). Monolayer graphenes (1LGs) were identified by optical microscopy (OM) and Raman spectroscopy. Copper phthalocyanine (CuPc) from Alfa-Aesar, Rhodamine 6G (R6G) from Sigma-Aldrich and Crystal Violet (CV) from Sinopharm Chemical Reagent Co., Ltd. were used as Raman probes directly as received. PMMA solid (996 K, from Sigma-Aldrich) was dissolved in ethyl lactate (5 wt%) for spin coating. Gold and silver films were deposited at a rate of about 1 Å/s, and at a pressure of about 10^{-3} Pa by vacuum thermal evaporation. All Raman spectra were obtained using a Horiba HR800 Raman system with a 632.8 nm He-Ne laser line, diameter of the laser spot is about 1 μm. All spectra in comparison were obtained under the same conditions if not specially pointed out. TEM characterizations of gold and silver films were carried out on a TEKNAI F20 equipment, the accelerating voltage is 200 kV. Samples were prepared by vacuum thermal evaporation of an 8-nm gold or silver film onto a copper grid (carbon covered). Three-dimensional-FDTD simulations were carried out by commercial software FDTD solutions 6.5 (Lumerical). The dielectric functions used to describe metal and graphene are from K. S. Novoselov, et al. (35, 36) for monolayer graphene and are from P. B. Johnson and R. W. Christy (37) for gold and silver.

1. Freudiger CW, et al. (2008) Label-free biomedical imaging with high sensitivity by stimulated Raman scattering microscopy. *Science* 322:1857–1861.
2. Fleischmann M, Hendra PJ, McQuillan AJ (1974) Raman spectra of pyridine adsorbed at a silver electrode. *Chem Phys Lett* 26:163–166.
3. Albrecht MG, Creighton JA (1977) Anomalously intense Raman spectra of pyridine at a silver electrode. *J Am Chem Soc* 99:5215–5217.
4. Jeanmaire DL, Van Duyne RP (1977) Surface Raman spectroelectrochemistry Part I. Heterocyclic, aromatic, and aliphatic amines adsorbed on anodized silver electrode. *J Electroanal Chem* 84:1–20.
5. Kneipp K, et al. (1997) Single molecule detection using surface-enhanced Raman scattering (SERS). *Phys Rev Lett* 78:1667–1670.
6. Nie SM, Emory SR (1997) Probing single molecules and single nanoparticles by surface-enhanced Raman scattering. *Science* 275:1102–1106.
7. Orrit M, Bernard J (1990) Single pentacene molecules detected by fluorescence excitation in a p-terphenyl crystal. *Phys Rev Lett* 65:2716–2719.
8. Otto A, Mrozek I, Grabhorn H, Akemann W (1992) Surface-enhanced Raman scattering. *J Phys Condens Matter* 4:1143–1212.
9. Schatz GC, Young MA, Van Duyne RP (2006) Electromagnetic mechanism of SERS. *Top Appl Phys* 103:19–46.
10. Le Ru EC, Etchegoin PG (2009) *Principles of Surface-Enhanced Raman Spectroscopy and related plasmonic effects* (Elservier, Amesterdam).
11. Jiang XD, Campion A (1987) Chemical effects in surface-enhanced Raman scattering: Pyridine chemisorbed on silver adatoms on Rh(100). *Chem Phys Lett* 140:95–100.
12. Udagawa M, Chou CC, Hemminger JC, Ushioda S (1981) Raman scattering cross section of adsorbed pyridine molecules on a smooth silver surface. *Phys Rev B* 23:6843–6846.
13. Li JF, et al. (2010) Shell-isolated nanoparticle-enhanced Raman spectroscopy. *Nature* 464:392–395.
14. Lin XM, Cui Y, Xu YH, Ren B, Tian ZQ (2009) Surface-enhanced Raman spectroscopy: substrate-related issues. *Anal Bioanal Chem* 394:1729–1745.
15. Freeman RG, et al. (1995) Self-assembled metal colloid monolayers: An approach to SERS substrates. *Science* 267:1629–1632.
16. Qin LD, et al. (2006) Designing, fabricating, and imaging Raman hot spots. *Proc Natl Acad Sci USA* 103:13300–13303.
17. Im H, Bantz KC, Lindquist NC, Haynes CL, Oh SH (2010) Vertically oriented sub-10-nm plasmonic nanogap arrays. *Nano Lett* 10:2231–2236.
18. Lim DK, Jeon KS, Kim HM, Nam JM, Suh YD (2010) Nanogap-engineerable Raman-active nanodumbbells for single-molecule detection. *Nat Mater* 9:60–67.
19. Lim DK, et al. (2011) Highly uniform and reproducible surface-enhanced Raman scattering from DNA-tailorable nanoparticles with 1-nm interior gap. *Nat Nanotechnol* 6:452–460.
20. Frens G (1973) Controlled nucleation for regulation of particle size in monodisperse gold suspensions. *Nature Phys Sci* 241:20–22.
21. Cooney RP, Mahoney MR, Howard MW (1980) Intense Raman spectra of surface carbon and hydrocarbons on silver electrodes. *Chem Phys Lett* 76:448–452.
22. Swathi RS, Sebastian KL (2008) Resonance energy transfer from a dye molecule to graphene. *J Chem Phys* 129:054703.
23. Xie LM, Ling X, Fang Y, Zhang J, Liu ZF (2009) Graphene as a substrate to suppress fluorescence in resonance Raman spectroscopy. *J Am Chem Soc* 131:9890–9891.
24. Wang YY, et al. (2010) Gold on graphene as a substrate for surface enhanced Raman scattering study. *Appl Phys Lett* 97:163111.
25. Ling X, et al. (2010) Can graphene be used as a substrate for Raman enhancement? *Nano Lett* 10:553–561.
26. Ling X, Zhang J (2010) First-layer effect in graphene-enhanced Raman scattering. *Small* 6:2020–2025.
27. Li XS, et al. (2009) Large-area synthesis of high-quality and uniform graphene films on copper foils. *Science* 324:1312–1314.
28. Jiao LY, et al. (2008) Creation of nanostructures with poly(methyl methacrylate)-mediated nanotransfer printing. *J Am Chem Soc* 130:12612–12613.
29. Fang Y, Seong NH, Dlott DD (2008) Measurement of the distribution of site enhancements in surface-enhanced Raman scattering. *Science* 321:388–392.
30. Cang H, et al. (2011) Probing the electromagnetic field of a 15-nanometre hotspot by single molecule imaging. *Nature* 469:385–388.
31. Cao YWC, Jin RC, Mirkin CA (2002) Nanoparticles with Raman spectroscopic fingerprints for DNA and RNA detection. *Science* 297:1536–1540.
32. Liu Z, et al. (2011) Revealing the molecular structure of single-molecule junctions in different conductance states by fishing-mode tip-enhanced Raman spectroscopy. *Nat Commun* 2:305.
33. Alvarez-Puebla RA, et al. (2011) Gold nanorods 3D-supercrystals as surface enhanced Raman scattering spectroscopy substrates for the rapid detection of scrambled prions. *Proc Natl Acad Sci USA* 108:8157–8161.
34. Novoselov KS, et al. (2004) Electric field effect in atomically thin carbon films. *Science* 306:666–669.
35. Kravets VG, et al. (2010) Spectroscopic ellipsometry of graphene and an exciton-shifted van Hove peak in absorption. *Phys Rev B* 81–155413.
36. Schedin F, et al. (2010) Surface-enhanced Raman spectroscopy of graphene. *ACS Nano* 4:5617–5626.
37. Johnson PB, Christy RW (1972) Optical constants of noble metals. *Phys Rev B* 6:4370–4379.

Xu et al.